

## Quantum heat transport of a two-qubit system: Interplay between system-bath coherence and qubit-qubit coherence

Akihito Kato and Yoshitaka Tanimura

Citation: *The Journal of Chemical Physics* **143**, 064107 (2015); doi: 10.1063/1.4928192

View online: <http://dx.doi.org/10.1063/1.4928192>

View Table of Contents: <http://scitation.aip.org/content/aip/journal/jcp/143/6?ver=pdfcov>

Published by the [AIP Publishing](#)

---

### Articles you may be interested in

[A qubit coupled with confined phonons: The interplay between true and fake decoherence](#)

*J. Chem. Phys.* **139**, 054103 (2013); 10.1063/1.4817303

[Entanglement dynamics of two qubits coupled individually to Ohmic baths](#)

*J. Chem. Phys.* **139**, 044115 (2013); 10.1063/1.4816122

[On the role of vibrational anharmonicities in a two-qubit system](#)

*J. Chem. Phys.* **131**, 034306 (2009); 10.1063/1.3152487

[Transport Properties and Control in Low-Dimensional Quantum Many-Body Systems \(abstract\)](#)

*AIP Conf. Proc.* **1119**, 240 (2009); 10.1063/1.3137875

[Analytic solution for entangled two-qubit in a cavity field](#)

*J. Math. Phys.* **45**, 4271 (2004); 10.1063/1.1795986

---



# Quantum heat transport of a two-qubit system: Interplay between system-bath coherence and qubit-qubit coherence

Akihito Kato<sup>a)</sup> and Yoshitaka Tanimura<sup>b)</sup>

*Department of Chemistry, Graduate School of Science, Kyoto University, Kyoto 606-8502, Japan*

(Received 23 June 2015; accepted 27 July 2015; published online 14 August 2015)

We consider a system consisting of two interacting qubits that are individually coupled to separate heat baths at different temperatures. The quantum effects in heat transport are investigated in a numerically rigorous manner with a hierarchical equations of motion (HEOM) approach for non-perturbative and non-Markovian system-bath coupling cases under non-equilibrium steady-state conditions. For a weak interqubit interaction, the total system is regarded as two individually thermostatted systems, whereas for a strong interqubit interaction, the two-qubit system is regarded as a single system coupled to two baths. The roles of quantum coherence (or entanglement) between the two qubits (q-q coherence) and between the qubit and bath (q-b coherence) are studied through the heat current calculated for various strengths of the system-bath coupling and interqubit coupling for high and low temperatures. The same current is also studied using the time convolutionless (TCL) Redfield equation and using an expression derived from the Fermi golden rule (FGR). We find that the HEOM results exhibit turnover behavior of the heat current as a function of the system-bath coupling strength for all values of the interqubit coupling strength, while the results obtained with the TCL and FGR approaches do not exhibit such behavior, because they do not possess the capability of treating the q-b and q-q coherences. The maximum current is obtained in the case that the q-q coherence and q-b coherence are balanced in such a manner that coherence of the entire heat transport process is realized. We also find that the heat current does not follow Fourier's law when the temperature difference is very large, due to the non-perturbative system-bath interactions. © 2015 AIP Publishing LLC. [<http://dx.doi.org/10.1063/1.4928192>]

## I. INTRODUCTION

Quantum heat transport phenomena exhibited by microscopic systems coupled to multiple macroscopic heat baths at different temperatures are of both fundamental and practical interest in quantum thermodynamics,<sup>1–18</sup> because such phenomena lie at the crossover between the macroscopic limit of quantum mechanics and microscopic limit of thermodynamics. Moreover, the advent of micro-technology allows us to investigate quantum heat current experimentally.<sup>19–21</sup> This leads us to consider the realistic possibility of developing devices that can control microscopic heat flow.<sup>22</sup> For this reason, understanding quantum heat transport phenomena is expected to play an important role in efforts to construct methods of efficient energy exploitation.

The well-established models of quantum heat transport phenomena consist of a chain of systems<sup>2–8</sup> or a single quantum system<sup>12–18</sup> coupled to two baths. The difficulty encountered in the study of such systems is due to problems involved in properly accounting for the system-bath coherence, which plays an essential role in quantum heat transport. Because full system-bath coherence can only be modeled with a non-perturbative and a non-Markovian treatment of the system-bath interaction, the perturbative quantum master equation approach cannot be applied. The modified Redfield and the polaron-transformed

master equations allow us to include nonperturbative effects, but there is an evidence that approaches employing these master equations lack accuracy in the strongly non-perturbative case.<sup>23,24</sup> Several methods involving the multi-configurational time-dependent Hartree (MCTDH) approach,<sup>14</sup> the quasi-adiabatic propagator path integral (QUAPI),<sup>17</sup> and Monte Carlo simulations<sup>16</sup> have been employed to investigate problems of this kind, but the applicability of such approaches is still limited. In the present study, we employ reduced hierarchical equations of motion (HEOM) to study the heat transport problem in order to treat a wide variety of physical conditions in a numerically rigorous manner under non-equilibrium steady-state conditions.<sup>25–39</sup> Moreover, we consider a two-qubit system<sup>40–43</sup> rather than a one-qubit system in order to increase the number of system degrees of freedom. This allows us to clearly demonstrate the role of system-bath coherence and system coherence in quantum heat transport processes.

The organization of this paper is as follows. In Sec. II, we present a model system of heat transfer and the definition of the heat current to be calculated. In Sec. III, we explain the hierarchical equations of motion approach in application to a system with two heat baths at different temperatures. To demonstrate the role of system-bath coherence, the time convolutionless (TCL) Redfield approach and the perturbative Fermi golden rule (FGR) approach are also introduced. In Sec. IV, numerical results obtained using the above three approaches are compared and discussed with respect to various values of the qubit-bath and qubit-qubit interactions. The effects of

<sup>a)</sup>Electronic mail: kato@kuchem.kyoto-u.ac.jp

<sup>b)</sup>Electronic mail: tanimura@kuchem.kyoto-u.ac.jp

the finite temperature difference on the heat current are also discussed. Section V is devoted to concluding remarks.

## II. MODEL

We employ a model consisting of two qubits described by the Hamiltonian

$$\hat{H}_k = \frac{\hbar\omega_k}{2} (\hat{\sigma}_z^k + \hat{I}_k), \quad (1)$$

for  $k = 1$  and  $2$ , where  $\hat{\sigma}_{x,y,z}^k$  and  $\hat{I}^k$  are the Pauli matrices and the unit matrix for the  $k$ th qubit, respectively. The interaction between the qubits is represented by

$$\hat{H}_{12} = \hbar J_{12} (\hat{\sigma}_+^1 \hat{\sigma}_-^2 + \hat{\sigma}_-^1 \hat{\sigma}_+^2). \quad (2)$$

Each qubit is coupled to its own heat bath,  $B_k$ . The total Hamiltonian is then given by

$$\hat{H}_{tot} = \sum_{k=1,2} (\hat{H}_k + \hat{H}_I^k + \hat{H}_B^k) + \hat{H}_{12}. \quad (3)$$

Here, the Hamiltonian of the  $k$ th heat bath and the interaction between the  $k$ th qubit and its heat bath are given by

$$\hat{H}_B^k = \sum_{j_k} \hbar\omega_{j_k} \hat{b}_{j_k}^\dagger \hat{b}_{j_k} \quad (4)$$

and

$$\hat{H}_I^k = \sum_{j_k} g_{j_k} \hat{\sigma}_x^k (\hat{b}_{j_k}^\dagger + \hat{b}_{j_k}), \quad (5)$$

where  $\omega_{j_k}$ ,  $g_{j_k}$ ,  $\hat{b}_{j_k}^\dagger$ , and  $\hat{b}_{j_k}$  are the frequency, coupling strength, creation operator, and annihilation operator for the  $j$ th mode of the  $k$ th bath, respectively. A schematic diagram of the total system is presented in Fig. 1. This model is useful to explore not only the role of quantum coherence (or entanglement) between the qubit and bath (q-b coherence) but also the role of that between the first and the second qubits (q-q coherence).

In the case of a weak q-b interaction, we regard each bath to be in its own thermal equilibrium state,  $e^{-\beta_k \hat{H}_B^k}$ , where  $\beta_k = 1/k_B T_k$  is the inverse temperature divided by the Boltzmann constant,  $k_B$  (see Fig. 2(a)). In the case of a strong q-b interaction, for small interqubit coupling  $J_{12}$ , each qubit and its bath are regarded as a single system characterized by the equilibrium state  $e^{-\beta_k (\hat{H}_k + \hat{H}_I^k + \hat{H}_B^k)}$  (see Fig. 2(b)), whereas for large  $J_{12}$ , the total system exists in a non-trivial thermal steady state, because q-b coherence between each qubit and its heat bath interfere through the q-q coherence. To investigate the interplay between the q-b coherence and the q-q coherence on heat transport, we must treat the entire system quantum mechanically in a consistent manner. Non-Markovian dynamics play a key role in this study, because a quantum mechanical

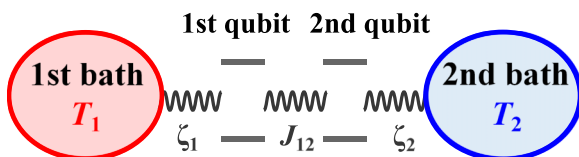
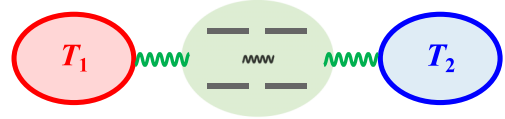


FIG. 1. Schematic depiction of the system consisting of two interacting qubits individually coupled to separate heat baths.

### (a) Redfield picture



### (b) Fermi Golden Rule picture

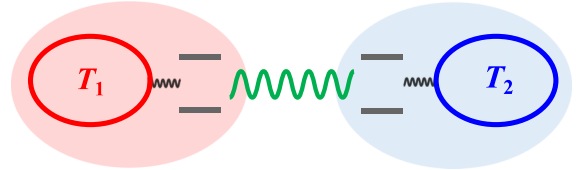


FIG. 2. Schematic depiction of the two limiting cases: (a) the Fermi golden rule approach, and (b) the Redfield approach. The green wavy lines indicate the parts of the interactions treated as perturbations in the respective approaches.

heat bath is by nature non-Markovian due to the time scale that arises as the inverse of the Matsubara frequency,  $\nu = 1/\beta\hbar$ . Due to the appearance of this time scale, the non-perturbative treatment of the system-bath interaction also becomes important even in the weak bath coupling case, because there will be multiple system-bath interactions that take place during the correlation time  $1/\nu$ .<sup>30–33</sup> For these reasons, conventional perturbative treatments involving the TCL Redfield approach cannot be applied to fully explore quantum effects in heat transport.

We define the heat current as the rate of change of the bath energy,

$$J_k \equiv -\frac{d\langle \hat{H}_B^k \rangle}{dt} = \frac{i}{\hbar} \langle [\hat{H}_B^k, \hat{H}_I^k] \rangle. \quad (6)$$

This definition is consistent with the thermodynamic definition in the equilibrium limit. From the stationarity condition,  $d\langle \hat{H}_I^k \rangle/dt = 0$ , the steady heat current can be evaluated as  $J_k = i\langle [\hat{H}_k + \hat{H}_{12}, \hat{H}_I^k] \rangle/\hbar$  in the non-equilibrium state. If the equation of motion for the reduced density operator of the system is written as  $d\hat{\rho}/dt = -i\hat{L}_S\hat{\rho} + \sum_{k=1,2} D_k[\hat{\rho}]$ , where  $\hat{L}_S\hat{\rho} = [\hat{H}_S, \hat{\rho}]/\hbar$ , with  $\hat{H}_S \equiv \hat{H}_1 + \hat{H}_2 + \hat{H}_{12}$  and  $D_k$  is the reduced operator from the  $k$ th bath, we can evaluate the heat current easily from the relation

$$J_k = -\text{tr} \{ (\hat{H}_k + \hat{H}_{12}) D_k[\hat{\rho}] \}. \quad (7)$$

We adapt the above expression to compute the heat current using the HEOM approach and the TCL Redfield approach. It should be noted that while  $\hat{H}_k + \hat{H}_{12}$  does not represent the internal energy of the  $k$ th qubit, the above expression is more convenient for numerical calculations than the expression defined in terms of two-body correlation functions of  $\hat{\sigma}_x^k$ .<sup>44–46</sup> Moreover, using the HEOM approach, we can study the heat current for any temperature difference between the baths with any strengths of the system-bath couplings under non-trivial equilibrium conditions, in which case the linear response theory for the thermal conductivity cannot be applied.

### III. NUMERICAL APPROACHES

#### A. HEOM approach

In this paper, we employ the reduced HEOM,<sup>25–33,36–39</sup> to calculate the heat current numerically in a rigorous manner under non-Markovian and non-perturbative conditions, specifically focusing on the roles of the q-b and q-q coherences. After eliminating the bath degrees of freedom, the effects of each bath are incorporated into the bath spectral density,  $I_k(\omega) \equiv \pi \sum_j g_{jk}^2 \delta(\omega - \omega_{jk})$ . The bath effects due to the  $k$ th bath are represented by the noise correlation function  $C_k(t)$ , written as

$$C_k(t) = \int_0^\infty \frac{d\omega}{\pi} I_k(\omega) \left[ \coth\left(\frac{\beta_k \hbar \omega}{2}\right) \cos(\omega t) - i \sin(\omega t) \right]. \quad (8)$$

We employ the Drude spectral distribution defined by

$$I_k(\omega) = \frac{\zeta_k \gamma_k^2 \omega}{\omega^2 + \gamma_k^2}, \quad (9)$$

where  $\zeta_k$  represents the coupling strength between the system and the  $k$ th bath, and  $\gamma_k$  corresponds to the cutoff frequency of the  $k$ th bath. Although the HEOM approach can treat various spectral distributions, including a Brownian one,<sup>34–36</sup> we chose the Drude form because it reduces to the standard Ohmic distribution for  $\gamma_k \rightarrow \infty$ . Also, there exist varieties of results for a single bath model with the Drude distribution, which can be helpful to analyze the present results. In the HEOM approach, we express the above function in terms of the exponential functions  $C_k(t) = \sum_{jk=0}^{jk=N_k} c_{jk} e^{-\gamma_{jk}|t|} + 2\Delta_k \delta(t)$ . Here, we use the Padé-based expression for  $c_{jk}$  and  $\gamma_{jk}$ ,<sup>37–39</sup> and  $N_k$  is an integer chosen such that the relation  $\sum_{jk=N_k+1}^{jk=\infty} c_{jk} e^{-\gamma_{jk}|t|} \approx 2\Delta_k \delta(t)$  holds. To properly account for the system-bath coherence for each of the baths, we need to introduce two sets of hierarchy elements, which we write as  $n_{j_1}$  and  $m_{j_2}$ .<sup>36</sup> Then, we obtain the following set of equations of motion for the reduced density operators by using the path integral method:

$$\begin{aligned} \hat{\rho}_{n_{j_1}, m_{j_2}} &= - \left[ i\hat{L}_S + \sum_{j_1} n_{j_1} \gamma_{j_1} + \sum_{j_2} m_{j_2} \gamma_{j_2} - \hat{\Xi} \right] \hat{\rho}_{n_{j_1}, m_{j_2}} \\ &\quad - \hat{\Phi}_1 \sum_{j_1} \hat{\rho}_{n_{j_1}^+, m_{j_2}} - \hat{\Phi}_2 \sum_{j_2} \hat{\rho}_{n_{j_1}, m_{j_2}^+} \\ &\quad - \sum_{j_1} n_{j_1} \hat{\Theta}_{j_1} \hat{\rho}_{n_{j_1}^-, m_{j_2}} - \sum_{j_2} m_{j_2} \hat{\Theta}_{j_2} \hat{\rho}_{n_{j_1}, m_{j_2}^-}, \end{aligned} \quad (10)$$

where  $\hat{\Theta}_{jk} = c'_{jk} \hat{\Phi}_k - c''_{jk} \hat{\Psi}_k$ ,  $\hat{\Xi} = \Delta_1 \hat{\Phi}_1^2 + \Delta_2 \hat{\Phi}_2^2$ ,

$$\hat{\Phi}_k \hat{\rho} \equiv \frac{i}{\hbar} (\hat{\sigma}_x^k \hat{\rho} - \hat{\rho} \hat{\sigma}_x^k), \quad (11)$$

and

$$\hat{\Psi}_k \hat{\rho} \equiv (\hat{\sigma}_x^k \hat{\rho} + \hat{\rho} \hat{\sigma}_x^k). \quad (12)$$

The constants  $c'_{jk}$  and  $c''_{jk}$  are the real and imaginary parts of  $c_{jk}$ , respectively. The indices  $n_{j_1}$  ( $m_{j_2}$ ) correspond to the effects of the first (second) bath, and  $n_{j_1}^+$  ( $n_{j_1}^-$ ) represents an increase (decrease) of the index  $n_{j_1}$  by 1. Note that the zeroth element,  $\hat{\rho}_{0,0}(t)$ , is identical to the actual reduced density operator of the system, and the remaining elements are the auxiliary density operators, which are introduced for the numerical calculation

and include nontrivial system-bath correlation effects. In the present case, we evaluate  $D_1[\hat{\rho}]$  in Eq. (7) for the first heat bath using the hierarchical members as

$$D_1[\hat{\rho}] = \Delta_1 \hat{\Phi}_1^2 \hat{\rho}_{0,0} - \hat{\Phi}_1 \sum_{j_1} \hat{\rho}_{0j_1}^+. \quad (13)$$

In principle, the HEOM provides an asymptotic approach that allows us to calculate various physical quantities with any desired accuracy by adjusting the number of hierarchical elements determined by  $N_k$ ; the error introduced by the truncation can be made negligibly small by choosing  $N_k$  to be sufficiently large. While we have to set larger  $N_k$  for lower temperature, we found that we can use smaller  $N_k$  by setting  $N_1 = N_2$  with suppressing numerical errors.

#### B. TCL Redfield approach

In the case of weak system-bath coupling,  $\zeta_{1,2} \ll J_{12}$ , the perturbative TCL Redfield approach is appropriate for calculating the heat current,<sup>33,49,50</sup> while we treat interqubit interactions non-perturbatively by explicitly treating the system degrees of freedom. In this case, the system consisting of the two qubits and the baths is weakly entangled because of the weak system-bath coupling. We express the eigenstate of the system Hamiltonian as  $\hat{H}_S|j\rangle = \hbar\bar{\omega}_j|j\rangle$ . The TCL Redfield equation for the reduced density matrix elements,  $\rho_{ij}(t) \equiv \langle i|\hat{\rho}_S(t)|j\rangle$ , is then given by<sup>49–51</sup>

$$\frac{\partial}{\partial t} \rho_{ij}(t) = -i\bar{\omega}_{ij} \rho_{ij}(t) + \sum_{k=1,2} \sum_{l,m} R_{ij,lm}^k(t) \rho_{lm}(t), \quad (14)$$

where  $\bar{\omega}_{ij} \equiv \bar{\omega}_i - \bar{\omega}_j$ , and  $R_{ij,lm}^k(t)$  is the Redfield tensor for the  $k$ th bath, defined as

$$\begin{aligned} R_{ij,lm}^k(t) &\equiv \Gamma_{mj,il}^k(t) + \Gamma_{li,jm}^{k\dagger}(t) \\ &\quad - \delta_{jm} \sum_n \Gamma_{in,nl}^k(t) - \delta_{il} \sum_n \Gamma_{jn,nm}^{k\dagger}(t), \end{aligned} \quad (15)$$

with

$$\begin{aligned} \Gamma_{ij,lm}^k(t) &= \bar{\Gamma}_{ijlm}^k \left( \frac{\zeta_k \gamma_k^2 e^{-i\frac{\beta_k \hbar \gamma_k}{2}}}{2 \sin\left(\frac{\beta_k \hbar \gamma_k}{2}\right)} \frac{1 - e^{-(\gamma_k + i\bar{\omega}_{lm})t}}{\gamma_k + i\bar{\omega}_{lm}} \right. \\ &\quad \left. - \frac{2}{\beta_k \hbar} \sum_{a_k=1}^{\infty} \frac{\zeta_k \gamma_k^2 \nu_{a_k}}{\gamma_k^2 - \nu_{a_k}^2} \frac{1 - e^{-(\nu_{a_k} + i\bar{\omega}'_{lm})t}}{\nu_{a_k} + i\bar{\omega}'_{lm}} \right). \end{aligned} \quad (16)$$

Here, the interaction tensor without the rotating wave approximation (RWA) is defined by

$$\bar{\Gamma}_{ijlm}^k \equiv \langle i|\hat{\sigma}_x^k|j\rangle \langle l|\hat{\sigma}_x^k|m\rangle. \quad (17)$$

In the Redfield case, the operator in Eq. (7) is expressed as

$$(D_1[\hat{\rho}])_{ij} = \sum_{l,m} R_{ij,lm}^1 \rho_{lm}. \quad (18)$$

While the positivity of reduced density operator is not maintained, we do not employ the RWA because it does not yield a proper steady state distribution, which is essential for calculating the heat flow.<sup>33</sup>

### C. Fermi golden rule approach

In the case of strong system bath coupling,  $\zeta_{1,2} \gg J_{12}$ , we can regard each system consisting of a qubit and its bath, with the Hamiltonian  $\hat{H}_k + \hat{H}_I^k + \hat{H}_B^k$ , as an extended bath. In this case,  $\hat{H}_{12}$  is the coupling between these extended baths. Then, we can treat  $\hat{H}_{12}$  perturbatively by invoking the FGR, assuming that the qubit systems are in the reduced equilibrium state of the  $k$ th qubit-plus-bath system described by  $\text{tr}_{B_k} \{e^{-\beta_k(\hat{H}_k + \hat{H}_I^k + \hat{H}_B^k)}\}$ , with temperature  $\beta_k$ . The resulting expression for the heat current is  $J = \hbar(\omega_1 \kappa_{1 \rightarrow 2} - \omega_2 \kappa_{2 \rightarrow 1})$ , where  $\kappa_{k \rightarrow k'}$  is the transition rate from the  $k$ th to the  $k'$ th qubit defined by

$$\kappa_{k \rightarrow k'} = 2J_{12}^2 \text{Re} \left[ \int_0^\infty dt E_k(t) A_{k'}(t) \right], \quad (19)$$

with the excitation and de-excitation functions  $E_k(t) = \text{tr}_{\text{tot}} \{ \langle g_k | \hat{\mu}_k(t) \hat{\rho}_{ee}^k \hat{\mu}_k | g_k \rangle \}$  and  $A_k(t) = \text{tr}_{\text{tot}} \{ \langle e_k | \hat{\mu}_k(t) \hat{\rho}_{gg}^k \hat{\mu}_k | e_k \rangle \}$  (for details, see the [Appendix](#)). Note that the form of the above transition rate is analogous to that of the exciton transfer rate in Förster theory.<sup>47,48</sup> Here,  $|e_k\rangle$  ( $|g_k\rangle$ ) is the excited (ground) state of the  $k$ th qubit,  $\hat{\mu}_k(t)$  is the Heisenberg operator,  $\hat{\mu}_k = |g_k\rangle \langle e_k| + |e_k\rangle \langle g_k|$ ,  $\hat{\rho}_{ee}^k$  ( $\hat{\rho}_{gg}^k$ ) is the total density matrix in the case that the  $k$ th qubit is in the excited (ground) state, and  $\text{tr}_{\text{tot}}\{\}$  is the trace over  $B_1 + B_2$  and the  $k'$  qubit degrees of freedom. In the present study, we determine  $E_k(t)$  and  $A_k(t)$  using the HEOM approach. The transition rates are determined by the correlation function of the operator  $\hat{\mu}_k = |g_k\rangle \langle e_k| + |e_k\rangle \langle g_k|$  in the local equilibrium state. To guarantee the validity of the local equilibrium assumption, in addition to the condition  $\zeta_{1,2} \gg J_{12}$ , we have to impose the condition that the two qubits are well separated, i.e.,  $J_{12} \ll \omega_{1,2}$ , as we elucidate on the basis of numerical results below.

## IV. NUMERICAL RESULTS

### A. Interplay between the q-q coherence and the q-b coherence

In the following, we set  $\omega_1 = \omega_2 = \omega$ ,  $\zeta_1 = \zeta_2$ , and  $\gamma_1 = \gamma_2 = 2\omega$ . The bath temperatures are characterized by the

average temperature,  $\bar{T} = (T_1 + T_2)/2$ , and the temperature difference,  $\Delta T = (T_1 - T_2)/2$ , where  $T_1 = 1/k_B\beta_1$  and  $T_2 = 1/k_B\beta_2$ . We consider (a) the high temperature case,  $\bar{T} = 2.0\hbar\omega/k_B$ , and (b) the low temperature case,  $\bar{T} = 0.2\hbar\omega/k_B$ , while we fix the difference between the bath temperatures with the small value  $\Delta T = 0.01\bar{T}$ . The heat current is evaluated from the thermal steady state. To obtain the steady state from the HEOM, we integrate Eq. (10) using the fourth-order Runge-Kutta method from a temporal initial state until all of the hierarchy elements reach the steady state. Then, we calculate the heat current from the first hierarchical members using Eq. (13). Similarly, the heat current in the TCL Redfield case is evaluated from Eq. (18) using the steady state solution of Eq. (14). In both HEOM and Redfield cases, the time step and the time duration of numerical integration are the same in the single bath case and the double bath case at all temperatures. Therefore, regardless of the temperature difference, the computational costs of the current calculations are similar. We display the results as functions of the effective coupling strength,  $\bar{\zeta} \equiv (\zeta_1 + \zeta_2)/J_{12}$ , for several values of  $J_{12}$  in Fig. 3. To elucidate the roles of the q-b and q-q coherences, we also calculated the heat current using the TCL Redfield approach without the RWA<sup>33,51</sup> and with the FGR approach using Eqs. (7) and (19).

We first discuss the high temperature case depicted in Fig. 3(a). Here, the noise is semi-classical and fluctuation and dissipation exhibit similar relaxation times.<sup>31–33</sup> In the weak interqubit coupling case,  $J_{12} = 0.01\omega$ , considered in Fig. 3(a-i), the curve obtained with the TCL approach nearly coincides with that obtained with the HEOM approach, because here the net coupling strength,  $\zeta_1 = \zeta_2 = J_{12}\bar{\zeta}$ , is small even in the case of large  $\bar{\zeta}$ , and hence, the perturbative treatment of the system-bath coupling is valid. The curve obtained with the FGR approach, by contrast, is close to the other curves only in the strong system-bath coupling regime, because we assumed that the qubit systems are in equilibrium states described by  $\text{tr}_{B_k} \{e^{-\beta_k(\hat{H}_k + \hat{H}_I^k + \hat{H}_B^k)}\}$  in the application of Eq. (19).

Next, we consider the case of intermediate and strong interqubit coupling, depicted in Figs. 3(a-ii) and 3(a-iii). It is seen that there is a large discrepancy between the TCL and HEOM results in the strong coupling region. This indicates

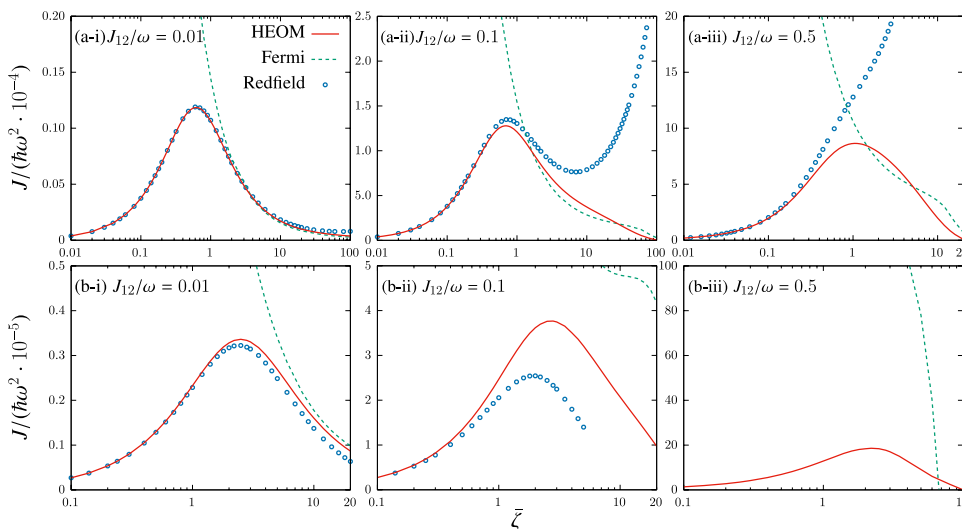


FIG. 3. Heat current calculated as functions of the effective coupling strength,  $\bar{\zeta} \equiv (\zeta_1 + \zeta_2)/J_{12}$ , is plotted in (a) the high temperature case,  $\bar{T} = 2.0\hbar\omega/k_B$ , and (b) the low temperature case,  $\bar{T} = 0.2\hbar\omega/k_B$ , for three values of the interqubit interaction,  $J_{12}/\omega$ : (i) 0.01, (ii) 0.1, and (iii) 0.5.

the failure of the perturbative treatment. The FGR results also deviate greatly from the HEOM results, because in this case, the qubit systems are not in their own equilibrium states,  $\text{tr}_{B_k} \{e^{-\beta_k(\hat{H}_k + \hat{H}_F^k + \hat{H}_B^k)}\}$ , but in non-trivial thermal steady states, due to the strong q-q coherence.

In the low temperature case depicted in Fig. 3(b), the fluctuation part of the noise exhibits highly non-Markovian behavior, and for this reason, a non-perturbative treatment of the noise is important even in the weak system-bath coupling case.<sup>32,33</sup> This explains the large discrepancy between the HEOM results and the TCL results in the intermediate and strong interqubit coupling region. In the cases of intermediate and strong interqubit coupling, the results obtained with the TCL approach do not converge, due to the breakdown of the positivity condition. The results obtained with the FGR approach deviate significantly from those obtained with the HEOM approach, because the two q-b coherences interfere significantly at low temperature, particularly for large interqubit coupling. This results in the entire system being in a non-trivial thermal steady state. Both in the high temperature and low temperature cases, the heat current increases as the interqubit coupling increases, because the interqubit coupling is the only pathway for the heat, as found by Yao in the case of a heat engine.<sup>52</sup> The current is large in the high temperature case even for the same value of  $J_{12}$ , due to the larger density of the heat energy at high temperature.

We found that for all values of the temperature and interqubit coupling strength considered here, the current exhibits turnover behavior as a function of the coupling strength. In the present case, heat transfer occurs through the coherence between the qubits even at high temperature.<sup>51</sup> To illustrate this point, in Fig. 4, we plot the density matrix elements for the transitions  $|e_1\rangle|g_2\rangle \rightarrow |g_1\rangle|e_2\rangle$  and  $|e_1\rangle|e_2\rangle \rightarrow |g_1\rangle|g_2\rangle$  for high and low temperatures, calculated using the HEOM approach. The similar tendency observed here for the heat current and  $\text{Im}\rho_{eg,ge}$  leads to the conclusion that the heat current occurs not through the population state but through the coherent state,  $|e_1\rangle|g_2\rangle \rightarrow |g_1\rangle|e_2\rangle$ . This situation can also be understood from

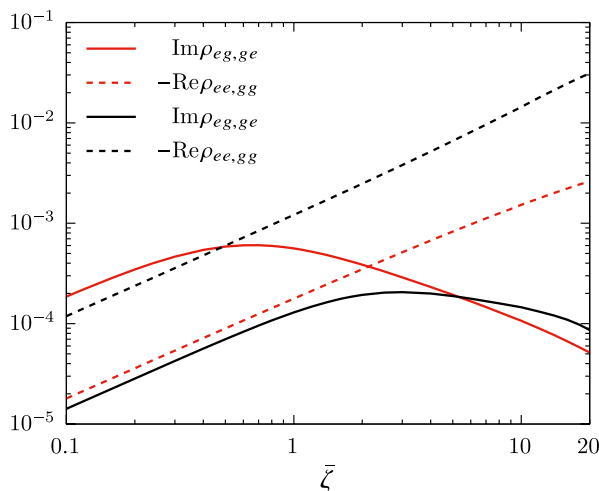


FIG. 4. The density matrix elements  $\text{Im}\rho_{eg,ge}$  (solid curves) and  $\text{Re}\rho_{ee,gg}$  (dashed curves) corresponding to the transitions  $|e_1\rangle|g_2\rangle \rightarrow |g_1\rangle|e_2\rangle$  and  $|e_1\rangle|e_2\rangle \rightarrow |g_1\rangle|g_2\rangle$ , respectively, are plotted for  $\bar{T} = 2.0\hbar\omega/k_B$  (red) and  $\bar{T} = 0.2\hbar\omega/k_B$  (black) in the intermediate coupling case,  $J_{12}/\omega = 0.1$ .

Eq. (7) if we replace  $\hat{H}_k + \hat{H}_{12}$  with  $\hat{H}_k$ ; the expression for the heat current is proportional to  $\text{Im}\rho_{eg,ge}$ .

In the weak system-bath coupling regime,  $\bar{\zeta} \ll 1$ , the current is an increasing function of  $\bar{\zeta}$ . This phenomenon can be interpreted as environment-assisted quantum transport (ENAQT),<sup>53,54</sup> in this case, the fluctuations that arise from the system-bath interaction supply the energy for the transition between qubits. In the strong system-bath coupling regime,  $\bar{\zeta} \gg 1$ ; however, the coherence is suppressed by dissipation that also arises from the system-bath interaction. The suppression of the transition rate is often referred to as the quantum Zeno effect, as can be understood if we regard the system-bath interaction to be a measurement of a microscopic quantum system carried out through use of a macroscopic instrument.

Surprisingly, as indicated by Fig. 3, the heat current is maximal near  $\bar{\zeta} \sim 1$  for any interqubit coupling. This indicates that heat transfer becomes most efficient when the b-q and q-q coherent processes are balanced in such a manner that coherence is realized for the total system. It should be noted that similar turnover behavior is observed in the chemical reaction problem,<sup>27,28,55</sup> electron transfer problem,<sup>34-36,56</sup> and exciton transfer problem,<sup>57</sup> but these are dynamical processes that occur through population transfer, whereas heat transfer is a steady-state process that occurs through coherence transfer.

## B. Effects of temperature difference: Deviation from Fourier's law

When the temperature difference between the two baths is small, the heat flow is characterized by the thermal conductance appearing in Fourier's law ( $J = \kappa\Delta T$ ), namely,  $\kappa \equiv \lim_{\Delta T \rightarrow 0} J/\Delta T$ . However, because there is quantum coherence between the system and the baths, the validity of Fourier's law in the quantum case is unclear. Because we introduced two heat baths with different temperatures in our formalism, we can test the limitation of Fourier's law. In Fig. 5, we depict the heat current as a function of the temperature differences,  $\Delta T$ , in (a) the high temperature case  $\bar{T} = 2.0\hbar\omega/k_B$  and (b) the low temperature case  $\bar{T} = 0.2\hbar\omega/k_B$  for the qubit-qubit interaction strength  $J_{12} = 0.1\omega$ . These two cases correspond to the cases in Figs. 3(a-ii) and 3(b-ii), respectively.

We find that when the temperature difference is small, the linear relation holds for all coupling strengths and average temperatures. For a large temperature difference, however, the simulation results deviate significantly from the value predicted by Fourier's law. Deviation was also observed when using the perturbative approach<sup>13</sup> and the polaron-transformed approach,<sup>18</sup> but the tendency of the deviation in the present case differs from that in those cases. Our results for the heat current are larger than those predicted by Fourier's law near the turnover region, while the results obtained with the perturbative and polaron-transformed approaches are smaller. Although we also found that the values obtained from our simulations become slightly smaller than those predicted by Fourier's law in both weak and strong system-bath coupling regions, the phenomena we observed are peculiar, because these phenomena depend on the qubit-bath and qubit-qubit interaction strengths as well as the temperature. This peculiarity

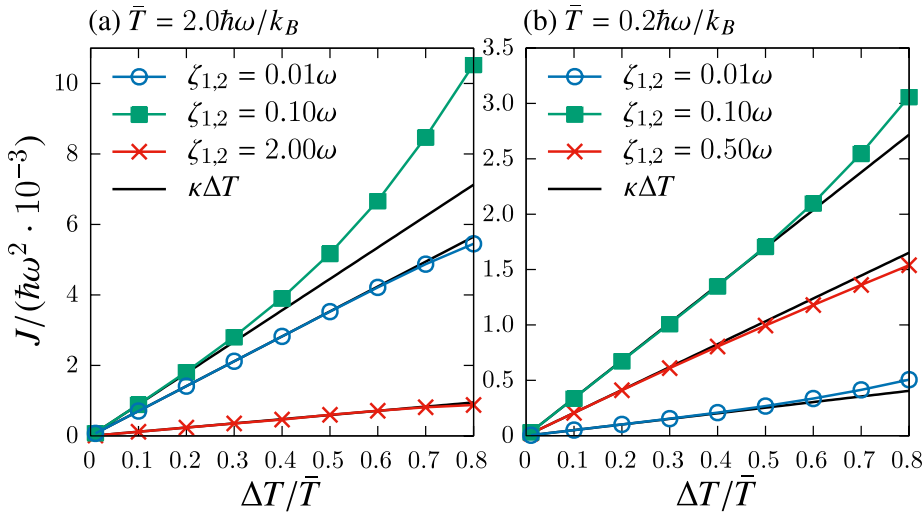


FIG. 5. Heat current calculated as a function of the temperature difference,  $\Delta T = (T_1 - T_2)/2$ , is plotted in (a) the high temperature case,  $\bar{T} = 2.0\hbar\omega/k_B$ , and (b) the low temperature case,  $\bar{T} = 0.2\hbar\omega/k_B$  for various values of the qubit-bath interaction  $\zeta_1 = \zeta_2$ .

is due to the non-perturbative system-bath interaction, and this seems to be the reason that it appears in the region, in which the perturbative Redfield approach breaks down. To properly account for the effects of the large temperature difference, we should introduce the second-order correction term as  $J = \kappa_1\Delta T + \kappa_2(\Delta T)^2 + \dots$ . As the Meir-Wingreen-like formula<sup>44,45</sup> suggested, this term arises from the quantum nature of the noise. Quantum coherence between the system and bath may also play a significant role in this correction term. To investigate further, analysis based on non-linear response functions should be carried out.<sup>59-61</sup>

## V. CONCLUDING REMARKS

In the present study, we calculated the heat current in a system consisting of two interacting qubits that are individually coupled to separate heat baths at different temperatures. We investigated the effects of the quantum coherence between the two qubits (q-q coherence) and between the qubits and baths (q-b coherence) on the heat current for various strengths of the system-bath coupling and interqubit coupling at high and low temperatures. We observed turnover behavior of the heat current as a function of the system-bath coupling strength, in which the heat current first increases as a function of this coupling strength, reaches a peak value, and then decreases. In the present study, we limited our analysis to the two-qubit case. By employing the numerical acceleration schemes developed for the HEOM approach, it is possible to investigate a longer chain of spins system<sup>4-8</sup> or a molecular junction system.<sup>9-11</sup> For example, using a graphics processing unit (GPU), we should be able to study the heat transport problem of 9-10 spins system.<sup>58</sup>

Although, here we restricted our analysis to the case of steady-state heat current, but there is no inherent restriction in the simulation of system dynamics when using the HEOM approach. Because in the present formalism, the difference between the temperatures of the two baths can be very large, we can study dynamical behavior of the heat current under highly non-equilibrium conditions, for example, in the case that one heat bath is in the high-temperature classical regime, while the other is in the low temperature quantum regime. Because the two-qubit model has been employed to study the

quantum information problem<sup>41,50,60-64</sup> and multidimensional spectroscopy,<sup>59</sup> we can characterize the present results in terms of dynamical behavior with respect to the results obtained in those studies. Heat engines and heat refrigerators<sup>65-69</sup> can also be studied by extending the present study. The investigation of these devices is left for future studies.

## ACKNOWLEDGMENTS

Financial support from a Grant-in-Aid for Scientific Research (No. A26248005) from the Japan Society for the Promotion of Science is acknowledged.

## APPENDIX: TRANSITION RATES IN THE FERMI GOLDEN RULE APPROACH

Here, we calculate the transition rate from the first to the second qubit,  $\kappa_{1 \rightarrow 2}$ . The rate from the second to the first,  $\kappa_{2 \rightarrow 1}$ , can be calculated in the same manner. We assume that the first qubit is initially in the excited state, while the second qubit is in the ground state, and hence, the state of the two-qubit system is given by  $|e_1\rangle|g_2\rangle$ . The probability of finding the two qubits in the state in which the excitation transfers from the first qubit to the second qubit, i.e.,  $|g_1\rangle|e_2\rangle$ , at time  $t$  is then expressed as

$$P(t) = \text{Tr}_B \left\{ \langle g_1 | \langle e_2 | e^{-i\hat{H}_{tot}t/\hbar} \hat{\rho}_0 e^{i\hat{H}_{tot}t/\hbar} |g_1\rangle |e_2\rangle \right\}, \quad (\text{A1})$$

where  $\hat{\rho}_0$  is the initial density operator of the total system without the qubit-qubit interaction. Expanding  $\hat{H}_{tot}$  appearing in Eq. (A1) in terms of  $\hat{H}_{12}$  to first order, the expression becomes

$$P(t) = \frac{1}{\hbar^2} \int_0^t d\tau \int_0^\tau d\tau' \text{Tr}_B \left\{ \langle g_1 | \langle e_2 | e^{i\hat{H}_0(\tau-\tau')/\hbar} \times \hat{H}_{12} e^{-i\hat{H}_0(\tau-\tau')/\hbar} \hat{\rho}_0 \hat{H}_{12} |g_1\rangle |e_2\rangle \right\}, \quad (\text{A2})$$

where  $\hat{H}_0 \equiv \hat{H}_{tot} - \hat{H}_{12}$ . The transition rate  $\kappa_{1 \rightarrow 2}$  is defined as the limit of the time derivative of the transition probability:  $\kappa_{1 \rightarrow 2} \equiv \frac{d}{dt} P(t)|_{t \rightarrow \infty}$ . Inserting the definition of  $\hat{H}_{12}$  into Eq. (A2), we obtain the expression given in Eq. (19). The above expression is identical to the transition rate obtained using exciton transfer theory.

- <sup>1</sup>Y. Dubi and M. Di Ventra, *Rev. Mod. Phys.* **83**, 131 (2011).
- <sup>2</sup>A. Dhar, *Adv. Phys.* **57**, 457 (2008).
- <sup>3</sup>J.-S. Wang, J. Wang, and J. T. Lü, *Eur. Phys. J. B* **62**, 381 (2008).
- <sup>4</sup>D. Segal, A. Nitzan, and P. Hänggi, *J. Chem. Phys.* **119**, 6840 (2003).
- <sup>5</sup>S. Lepri, R. Livi, and A. Politi, *Phys. Rep.* **377**, 1 (2003).
- <sup>6</sup>A. Bermudez, M. Bruderer, and M. B. Plenio, *Phys. Rev. Lett.* **111**, 040601 (2013).
- <sup>7</sup>A. Ruiz, D. Alonso, M. B. Plenio, and A. del Campo, *Phys. Rev. B* **89**, 214305 (2014).
- <sup>8</sup>N. Li and B. Li, *AIP Adv.* **2**, 041408 (2012).
- <sup>9</sup>M. Galperin, A. Nitzan, and M. A. Ratner, *Phys. Rev. B* **75**, 155312 (2007).
- <sup>10</sup>A. Buldum, D. M. Leitner, and S. Ciraci, *Europhys. Lett.* **47**, 208 (1999).
- <sup>11</sup>D. M. Leitner, *J. Phys. Chem. B* **117**, 12820 (2013).
- <sup>12</sup>D. Segal and A. Nitzan, *Phys. Rev. Lett.* **94**, 034301 (2005).
- <sup>13</sup>D. Segal, *Phys. Rev. B* **73**, 205415 (2006).
- <sup>14</sup>K. A. Velizhanin, H. Wang, and M. Thoss, *Chem. Phys. Lett.* **460**, 325 (2008).
- <sup>15</sup>T. Ruokola and T. Ojanen, *Phys. Rev. B* **83**, 045417 (2011).
- <sup>16</sup>K. Saito and T. Kato, *Phys. Rev. Lett.* **111**, 214301 (2013).
- <sup>17</sup>N. Boudjada and D. Segal, *J. Phys. Chem. A* **118**, 11323 (2014).
- <sup>18</sup>C. Wang, J. Ren, and J. Cao, e-print [arXiv:1410.4366](https://arxiv.org/abs/1410.4366).
- <sup>19</sup>D. G. Cahill, W. K. Ford, K. E. Goodson, G. D. Mahan, A. Majumdar, H. J. Maris, R. Merlin, and S. R. Phillpot, *J. Appl. Phys.* **93**, 793 (2003).
- <sup>20</sup>N. Yang, X. Xu, G. Zhang, and B. Li, *AIP Adv.* **2**, 041410 (2012).
- <sup>21</sup>A. M. Marconnet, M. A. Panzer, and K. E. Goodson, *Rev. Mod. Phys.* **85**, 1295 (2013).
- <sup>22</sup>N. Li, J. Ren, L. Wang, G. Zhang, P. Hänggi, and B. Li, *Rev. Mod. Phys.* **84**, 1045 (2012).
- <sup>23</sup>H.-T. Chang, P.-P. Zhang, and Y.-C. Cheng, *J. Chem. Phys.* **139**, 224112 (2013).
- <sup>24</sup>Y. Chang and Y.-C. Cheng, *J. Chem. Phys.* **142**, 034109 (2015).
- <sup>25</sup>Y. Tanimura and R. Kubo, *J. Phys. Soc. Jpn.* **58**, 101 (1989).
- <sup>26</sup>Y. Tanimura, *Phys. Rev. A* **41**, 6676 (1990).
- <sup>27</sup>Y. Tanimura and P. G. Wolynes, *Phys. Rev. A* **43**, 4131 (1991).
- <sup>28</sup>Y. Tanimura and P. G. Wolynes, *J. Chem. Phys.* **96**, 8485 (1992).
- <sup>29</sup>A. Ishizaki and Y. Tanimura, *J. Phys. Soc. Jpn.* **74**, 3131 (2005).
- <sup>30</sup>Y. Tanimura, *J. Phys. Soc. Jpn.* **75**, 082001 (2006).
- <sup>31</sup>A. Kato and Y. Tanimura, *J. Phys. Chem. B* **117**, 13132 (2013).
- <sup>32</sup>Y. Tanimura, *J. Chem. Phys.* **141**, 044114 (2014).
- <sup>33</sup>Y. Tanimura, *J. Chem. Phys.* **142**, 144110 (2015).
- <sup>34</sup>M. Tanaka and Y. Tanimura, *J. Phys. Soc. Jpn.* **78**, 073802 (2009).
- <sup>35</sup>M. Tanaka and Y. Tanimura, *J. Chem. Phys.* **132**, 214502 (2010).
- <sup>36</sup>Y. Tanimura, *J. Chem. Phys.* **137**, 22A550 (2012).
- <sup>37</sup>J. Hu, R.-X. Xu, and Y. J. Yan, *J. Chem. Phys.* **133**, 101106 (2010).
- <sup>38</sup>J. Hu, M. Luo, F. Jiang, R.-X. Xu, and Y. J. Yan, *J. Chem. Phys.* **134**, 244106 (2011).
- <sup>39</sup>J.-J. Ding, J. Xu, J. Hu, R.-X. Xu, and Y. J. Yan, *J. Chem. Phys.* **135**, 164107 (2011).
- <sup>40</sup>T. Yu and J. H. Eberly, *Phys. Rev. Lett.* **93**, 140404 (2004).
- <sup>41</sup>B. Bellomo, R. LoFranco, and G. Compagno, *Phys. Rev. Lett.* **99**, 160502 (2007).
- <sup>42</sup>A. Sergi, I. Sinayskiy, and F. Petruccione, *Phys. Rev. A* **80**, 012108 (2009).
- <sup>43</sup>E. Ferraro, M. Scala, R. Migliore, and A. Napoli, *Phys. Rev. A* **80**, 042112 (2009).
- <sup>44</sup>T. Ojanen and A.-P. Jauho, *Phys. Rev. Lett.* **100**, 155902 (2008).
- <sup>45</sup>K. A. Velizhanin, M. Thoss, and H. Wang, *J. Chem. Phys.* **133**, 084503 (2010).
- <sup>46</sup>K. Saito, *Europhys. Lett.* **83**, 50006 (2008).
- <sup>47</sup>V. May and O. Kühn, *Charge and Energy Transfer Dynamics in Molecular Systems* (Wiley-VCH, 2011).
- <sup>48</sup>S. Jang and Y.-C. Cheng, *WIREs Comput. Mol. Sci.* **3**, 84 (2013).
- <sup>49</sup>M. Ban, S. Kitajima, and F. Shibata, *Phys. Lett. A* **374**, 2324 (2010).
- <sup>50</sup>H. P. Breuer and F. Petruccione, *The Theory of Open Quantum Systems* (Oxford University Press, New York, 2002).
- <sup>51</sup>H. Wichterich, M. J. Henrich, H.-P. Breuer, J. Gemmer, and M. Michel, *Phys. Rev. E* **76**, 031115 (2007).
- <sup>52</sup>Y. Yao, *Phys. Rev. B* **91**, 045421 (2015).
- <sup>53</sup>M. B. Plenio and S. F. Huelga, *New J. Phys.* **10**, 113019 (2008).
- <sup>54</sup>P. Rebentrost, M. Mohseni, I. Kassal, S. Lloyd, and A. Aspuru-Guzik, *New J. Phys.* **11**, 033003 (2009).
- <sup>55</sup>M. Topaler and N. Makri, *J. Chem. Phys.* **101**, 7500 (1994).
- <sup>56</sup>M. Topaler and N. Makri, *J. Phys. Chem.* **100**, 4430 (1996).
- <sup>57</sup>A. Ishizaki and G. R. Fleming, *J. Chem. Phys.* **130**, 234110 (2009).
- <sup>58</sup>M. Tsuchimoto and Y. Tanimura, *J. Chem. Theory Comput.* **11**, 3859 (2015).
- <sup>59</sup>Y. Tanimura and A. Ishizaki, *Acc. Chem. Res.* **42**, 1270 (2009).
- <sup>60</sup>A. G. Dijkstra and Y. Tanimura, *Phys. Rev. Lett.* **104**, 250401 (2010).
- <sup>61</sup>A. G. Dijkstra and Y. Tanimura, *J. Phys. Soc. Jpn.* **81**, 063301 (2012).
- <sup>62</sup>W. K. Wootters, *Phys. Rev. Lett.* **80**, 2245 (1998).
- <sup>63</sup>L. Quiroga, F. J. Rodriguez, M. E. Ramirez, and R. Paris, *Phys. Rev. A* **75**, 032308 (2007).
- <sup>64</sup>L.-A. Wu and D. Segal, *Phys. Rev. A* **84**, 012319 (2011).
- <sup>65</sup>R. Kosloff and A. Levy, *Annu. Rev. Phys. Chem.* **65**, 365 (2014).
- <sup>66</sup>L. A. Correa, J. P. Palao, D. Alonso, and G. Adesso, *Sci. Rep.* **4**, 3949 (2014).
- <sup>67</sup>M. O. Scully, K. R. Chapin, K. E. Dorfman, M. B. Kim, and A. Svidzinsky, *Proc. Natl. Acad. Sci. U. S. A.* **108**, 15097 (2011).
- <sup>68</sup>G. Benenti, G. Casati, T. Prosen, and K. Saito, e-print [arXiv:1311.4430](https://arxiv.org/abs/1311.4430).
- <sup>69</sup>D. Gelbwaser-Klimovsky, W. Niedenzu, and G. Kurizki, e-print [arXiv:1503.01195](https://arxiv.org/abs/1503.01195).